Colloids and Surfaces A: Physicochemical and Engineering Aspects 714 (2025) 136544

Contents lists available at ScienceDirect

Colloids and Surfaces A: Physicochemical and Engineering Aspects

journal homepage: www.elsevier.com/locate/colsurfa

Optimizing *Lavandula mairei*-mediated silver nanoparticle synthesis for effective inhibition and eradication of multidrug-resistant bacterial biofilms

Soufiane EL Megdar [a,b], Asma Laktib [a], Raja Elkheloui [a], Hicham Abou Oualid [c], Camelia Filofteia Diguţă [d], Florentina Matei [d,e], Sophie C. Gangloff [b], Fany Reffuveille [b], Fouad Msanda [f], Mohamed Hassi [a], Fatima Hamadi [a,*]

[a] Laboratory of Microbial Biotechnology and Plants Protection. Biology Department. Sciences Faculty, Ibn Zohr University, Agadir 80000, Morocco
[b] Université de Reims Champagne Ardenne, UFR de Pharmacie, UR Biomatériaux et Inflammation en Site Osseux (URBIOS), Reims 51100, France
[c] Green Energy Park, IRESEN–UM6P, 43153 Benguerir, Morocco
[d] Faculty of Biotechnologies, University of Agronomic Sciences and Veterinary Medicine Bucharest, 59 Mărăşti Blvd., District 1, Bucharest 011464, Romania
[e] Faculty of Food Industry and Tourism, Transilvania University of Braşov, 148 Castelului St., Braşov 500014, Romania
[f] Laboratory of Biotechnologies and Valorization of Natural Resources, Biology Department. Sciences Faculty, Ibn Zohr University, Agadir 80000, Morocco

GRAPHICAL ABSTRACT

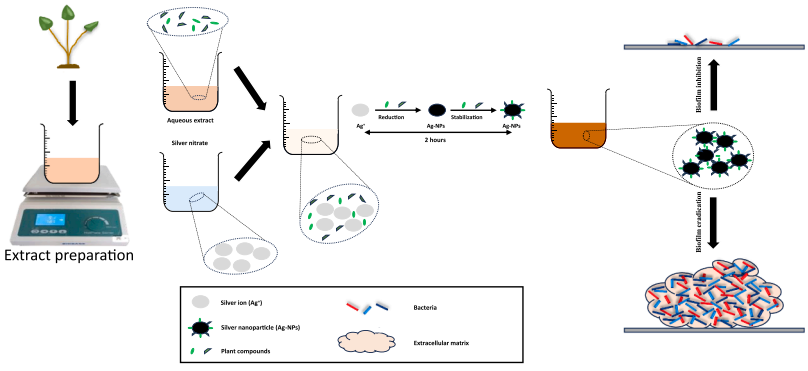

ARTICLE INFO

Keywords:
Silver nanoparticles
Multidrug-resistant bacteria
Biofilm inhibition
Biofilm eradication
Lavandula mairei, green synthesis, ESBL-producing Enterobacteriaceae

ABSTRACT

Multi-resistant bacteria represent a significant public health threat, due to their resistance to many antibiotics and their biofilm formation capacity, which are difficult to treat and often lead to prolonged illness. Silver nanoparticles are promising antimicrobial agents, penetrating biofilms and serving as potential antimicrobial agents against multi-drug resistant bacteria. This study focuses on optimizing the silver nanoparticle synthesis based on the extract of *Lavandula mairei*. The effects of silver nitrate concentration, extract volume, reaction time and temperature were investigated. In addition, the nanoparticles were characterized by UV–vis spectroscopy, X-ray diffraction, scanning electron microscopy, energy dispersive X-ray spectroscopy, Fourier transform infrared spectroscopy, and dynamic light analysis. The synthesized nanoparticles were subsequently evaluated for inhibiting and eradicating biofilms formed by multi-resistant strains including *Acinetobacter baumannii* and ESBL-producing and non-ESBL-producing Enterobacteriaceae. Silver nanoparticles were successfully synthesized,

* Corresponding author.
E-mail address: f.hamadi@uiz.ac.ma (F. Hamadi).

https://doi.org/10.1016/j.colsurfa.2025.136544
Received 2 September 2024; Received in revised form 6 February 2025; Accepted 28 February 2025
Available online 7 March 2025

exhibiting a crystalline structure that was predominantly spherical, with sizes ranging from 30 to 60 nm at the optimum reaction time of 2 hours. They also showed a high silver content and retained functional groups from the plant extract. Additionally, dynamic light scattering revealed a bimodal size distribution, with peaks at 25.10 nm and 124.47 nm. Furthermore, the percentage of biofilm inhibition ranged from 36.33 ± 0.89–80.07 ± 1.31 % at a sub-minimum inhibitory concentration, while the rate of biofilm eradication ranged from 28.04 ± 1.60–71.95 ± 1.99 %. This research addresses the urgent need for new antimicrobial strategies and highlights the promise of biological silver nanoparticles as efficient agents against biofilm-associated bacterial resistance.

1. Introduction

Presently, there is an increasing apprehension over antimicrobial resistance, since some organisms demonstrate resistance to a broad spectrum of antibiotics [1,2]. The presence of this resistance in bacterial infections is strongly linked to higher rates of illness and death. In 2021, bacterial resistance to antibiotics was associated with 4.71 million deaths worldwide, among which 1.14 million were directly due to infections caused by drug-resistant bacteria (MDR). In the absence of effective interventions, this number is expected to rise to 8.22 million deaths per year by 2050 [3]. The intricate mechanisms of multidrug resistance reported in both Gram-negative and Gram-positive bacteria provide difficulties in treatment and may render them impervious to traditional antibiotics [1]. Bacterial resistance to β-lactam antibiotics, driven by the production of β-lactamases such as extended-spectrum β-lactamases (ESBLs) and carbapenemases, poses a critical global health challenge. These enzymes hydrolyze the β-lactam ring of the antibiotic, resulting in antibiotic resistance [4]. According to the WHO [5] report, third-generation cephalosporin-resistant Enterobacterales and carbapenem-resistant strains, such as *Acinetobacter baumannii (A. baumannii)*, are particularly concerning. These pathogens are associated with high mortality rates, especially in low- and middle-income countries, underscoring the urgent need for innovative strategies to address these infections [5]. It has also been demonstrated that the mortality rate of patients infected with *A. baumannii* in intensive care units is between 45 % and 60 %, and can exceed 80 % in cases of drug resistance [6]. In addition to these intricate resistance mechanisms, the development of biofilms exacerbates the difficulty of the approach.

Biofilm constitutes an organized assembly of bacteria enveloped within a self-generated polymer matrix comprising polysaccharides, proteins, and extracellular DNA [1]. Bacterial biofilms exhibit notable resistance to antibiotics, disinfectant, chemicals and also to processes like phagocytosis and other elements of the body's inflammatory defense system [7,8]. Bacteria capable of forming biofilms represent a major threat to human health, being implicated in 65–80 % of infections, particularly those that persist over time [9]. Biofilm production is a frequently used survival strategy by bacteria that are resistant to many drugs, such as some strains of Extended spectrum β-lactamase (ESBL)-producing Enterobacteriaceae[10] and *A. baumannii* [11]. Bacterial biofilms, particularly those produced by *A. baumannii*, have become a significant issue in hospital environments [9]. A study revealed that 65.63 % of *A baumannii* clinical isolates formed biofilms, with 41.34 % classified as strong producers, 33.57 % as moderate, and 27.63 % as weak. These strains were most prevalent in the Western Pacific, followed by Asia and Africa [6]. *A. baumannii*, characterized as a Gram-negative bacterium, has notably gained recognition for its efficient adhesion of medical surfaces and devices. The capacity of this organism to create strong biofilms not only allows infections to persist but also presents a substantial danger due to its growing resistance to several antimicrobial medications [11]. In addition, ESBL-producing Enterobacteriaceae further exacerbate the danger through their capacity for robust biofilm formation. The incidence of ESBL-producing Enterobacteriaceae has seen a substantial rise in the last decade, emerging as a global public health issue of growing concern, due to their increased ability to establish resistant biofilms [12]. In France, the incidence density of infections caused by these bacteria is approximately three times higher than that of methicillin-resistant *Staphylococcus aureus* [13]. In this context, there is an increasing need for alternatives to conventional antibiotics to meet the challenge of antibiotic resistance and limit biofilm-related diseases.

In recent decades, significant attention has been given to the research and biomedical evaluation of metallic nanoparticles derived from noble metals. This is due to their distinctive chemical, biological, and physical properties [14]. Nanoscale materials show distinct properties compared to bulk ones, mainly as a result of the higher surface-to-volume ratio [14]. In the realm of metallic nanoparticles, silver nanoparticles (Ag-NPs) find extensive applications as agents with anticancer, antibacterial, antifungal, antiviral, and anti-inflammatory properties. Furthermore, they serve as drug delivery agents and are employed in medical devices for the diagnosis and detection of various diseases [15]. Ag-NPs may be produced in several ways, such as chemical, physical, and biological methods. Among these, the utilization of biological substances holds a distinct advantage over alternative methods, as it is ecological and does not generate toxic byproducts [16]. The eco-friendly approach to synthesizing nanoparticles involves utilizing biological entities like algae, plant materials, microbes, and similar resources. This strategy has several advantages, such as its characteristic of being a single-step procedure that produces nanoparticles characterized by stability, cost-effectiveness, and particular dimensions [16]. In addition to the advantages of the eco-friendly approach, the synthesis of silver nanoparticles is highly dependent on several critical parameters. Among these, key factors such as temperature, reaction time, concentration of metal precursors and volume of biological reducing agents significantly influence the size, shape, and stability of the nanoparticles [17].The utilization of plant materials in eco-friendly nanoparticle synthesis presents notable advantages, compared to synthesizing nanoparticles using microbes, which may be difficult owing to the complexity involved in storing, isolating, and maintaining microorganisms [18], In contrast, the plant-based method uses various secondary metabolites found in plant extracts, including polysaccharides, terpenoids, phenolics, tannins, saponins, alkaloids, and flavones. The presence of these chemicals facilitates the efficient reduction and stabilization of nanoparticles [19]. This mechanism is further elucidated by Vanlalveni et al. [20]. who suggested that the oxidation of various biomolecules like tannins, carboxylic acids, ketones, flavonoids, aldehydes, and plant come to be primarily involved in the reduction of silver ions to metallic silver [20].

The Lavandula L. genus, belonging to the Lamiaceae family, is indigenous to the Mediterranean region, India, and the Canary Islands. Currently, it is under cultivation in various parts of the globe [21,22]. The Lavandula genus is present in the Moroccan flora with nine species and subspecies, among which five are endemic. Among the endemic lavenders, *Lavandula mairei* Humbert (*L. mairei*) is categorized as a scarce species [23]. It is a perennial shrub, typically reaching heights of 0.40–0.80 m, adorned with striking violet flower spikes. *L. mairei* finds extensive application in traditional medicine for addressing diverse health concerns, including gastrointestinal ailments, asthma, cough, and microbial infections, with notable efficacy in inhibiting biofilm formation [24,25]. It is precisely for these reasons that we have chosen *L. mairei* as the subject of our study. Notably, no previous studies have

focused on the antibiofilm activity of Ag-NPs synthesized using *L. mairei*.

To fill that knowledge gap, our research aims to contribute valuable insights into the potential of *L. mairei* as a novel and unexplored source of Ag-NPs synthesis. Consequently, the primary aims of our research are to optimize the conditions for the synthesis of silver nanoparticles using *L. mairei*. Subsequently, we aim to conduct a thorough characterization of the nanoparticles and determine their MIC and minimum bactericidal concentration (MBC). Additionally, we seek to evaluate their capacity to inhibit and eradicate biofilms formed by multidrug-resistant bacterial strains, such as *A. baumannii* and Enterobacteriaceae, both ESBL-producing and non-ESBL-producing.

2. Materials and methods

2.1. Bacterial strains

In the laboratory, bacterial strains were isolated from surfaces and medical instruments in a hospital intensive care unit in Morocco. [26]. Among them were seven Enterobacteriaceae strains, including five ESBL-producing strains: *E. coli* 2, *E. coli* 3, *K. pneumoniae* 2, *K. pneumoniae* 4, and *E. hormaechei* [27], as well as two non-ESBL-producing strains: *E. cloacae* and *K. pneumoniae* 9 (Table A, Appendices). In addition, ten multidrug-resistant strains of *A. baumannii* have been identified [21]. The bacterial strains were incubated on Tryptic Soy Agar (TSA, Biokar Diagnostics) for 24 hours at 37°C.

2.2. Preparation of plant extract

The extraction was performed according to the method outlined by Qais et al. [28] with slight modifications. Briefly, five grams of plant powder were added to 100 mL of distilled water. After that, the whole was then heated at 90°C for 30 minutes. Once the mixture had cooled, the extract was filtered and stored for future use [28].

2.3. Optimization of green synthesis of Ag-NPs

In the pursuit of enhancing nanoparticle efficacy, it is crucial to optimize the conditions that influence the biosynthesis of these nanoparticles from *L. mairei*. Ag-NPs were synthesized according to Qais et al. [28] with partial modifications. Different volumes of the aqueous extract of *L. mairei* were mixed with varying concentrations of silver nitrate at different incubation times and temperatures. The resultant mixture was subjected to centrifugation at 10,000 rpm for 30 minutes to extract the nanoparticles from the reaction mixture. The resulting pellet was then repeatedly washed with distilled water to eliminate impurities. Following this, the nanoparticle pellet was then dried at 50°C to remove traces of water and obtain a powder. The obtained Ag-NPs powder was then stored at 4°C for subsequent analyses [28].

2.3.1. Influence of aqueous extract volume on the silver nanoparticles synthesis

The impact of extract volume on nanoparticle synthesis was investigated by mixing 0.50, 1, 2, 4, and 8 mL of the extract with 20 mL of silver nitrate. This parameter variation aimed to clarify the relationship between extract volume and Ag-NPs production. UV–visible spectroscopy was used to compare the absorption spectra and investigate the nanoparticle formation process.

2.3.2. Influence of silver nitrate concentration on silver nanoparticles synthesis

Under constant volume conditions (20 mL), three concentrations of silver nitrate (0.25, 0.50, and 1 mM) were used to investigate the impact of this concentration on the Ag-NPs production. This experiment aims to determine the impact of different silver nitrate concentrations on nanoparticle formation. UV–vis spectroscopy analysis was used to analyze biosynthesized Ag-NPs that were biosynthesized.

2.3.3. Influence of reaction temperature on silver nanoparticles synthesis

To assess how temperature affects Ag-NPs biosynthesis, the nanoparticle synthesis process was conducted at different temperatures (25°C, 40°C, 50°C, and 70°C). Ag-NPs production was examined using UV–vis spectroscopy.

2.3.4. Influence of reaction time on silver nanoparticles synthesis

Incubation time impact on nanoparticle synthesis was examined using various times of reaction (0, 2, 4, 6 and 8 hours), and the formed Ag-NPs were analyzed using UV–vis spectroscopy.

2.4. Characterization of synthesized nanoparticles

2.4.1. UV–vis spectral analysis

A UV–vis spectrophotometer, specifically the GENESYS 50 (Thermo Fisher Scientific, USA), was employed to characterize the Ag-NPs in their preliminary phases. Analysis of the UV–vis spectra of the synthesis solutions indicated the reduction of silver ions to silver nanoparticles. Absorbance spectra (350–800 nm) of the biosynthesized Ag-NPs solution were measured using this instrument [29].

2.4.2. Scanning electron microscopy (SEM)

SEM imaging was employed for investigating the nanoparticles' morphology. Samples were coated with a thin layer of gold using a sputtering device to improve conductivity and minimize charging effects [30]. SEM imaging was performed using a (JEOL JSM IT-100 Tokyo, Japan) scanning electron microscope from Ibn Zohr University. This technique was used to analyze the size, and shape of biosynthesized nanoparticles at different times, in particular at 2, 4, 6 and 8 h from synthesis, in order to determine changes in nanoparticle size and morphology over time.

2.4.3. Energy dispersive X-ray spectroscopy analysis (EDS)

The basic composition of the resulting Ag-NPs was analyzed by energy dispersive X-ray spectrometry. This approach makes it possible to identify and quantify the elements present in biosynthesized nanoparticles. EDS analyses were carried out using a (JEOL JSM IT-100 Tokyo, Japan) scanning electron microscope with an JEOL-made EDS, revealing important details about the chemical composition and purity of the sample [30].

2.4.4. X-ray diffraction (XRD)

XRD analysis was carried out following the method of Qais et al. [28], with slight modifications. Briefly, a Bruker D8 Advance Twin diffractometer (Bruker Corporation, Germany) equipped with Cu Kα radiation (λ = 1.5404 Å), was used to scan the 2θ domain of 10° to 100°. This analysis was used to examine the crystal structure of the synthesized nanoparticles [28].

The Debye-Scherrer equation was applied to calculate the powder crystal size of Ag-NPs [31]:

$$D = k\lambda / \beta \cos\theta \quad (1)$$

where D = crystallite size (nm), K = Scherer constant (K = 0.94), λ = X-ray diffraction wavelength of Cu Ka radiation, β = half-width of the peak, and θ = the angle of diffraction.

2.4.5. Fourier Transform Infrared Spectroscopy Analysis (FTIR)

FTIR analysis was used to identify the functional groups involved in the green synthesis of Ag-NPs, characterizing both the synthesized Ag-NPs and the plant extract within a wavenumber range of 4400–450 cm^{-1} [32].

2.4.6. Dynamic light scattering (DLS) analysis

Nanoparticles size distribution was carried out using a Zeta sizer dynamic light scattering detector (Malvern Panalytical, UK). A small

quantity of synthesized Ag-NPs was dispersed in water and sonicated for five seconds to ensure the solution's homogeneity. The solution was diluted many times and analyzed at 25 °C until a clear size distribution as a function of intensity was produced.

2.5. Antibacterial activity of silver nanoparticles using the microdilution method

The MIC was determined according to the protocol outlined [33] with minor modifications. Initially, a bacterial suspension was established from a fresh overnight bacterial culture and adjusted to a 0.5 McFarland standard, equivalent to approximately ~1.50 × 10^8 CFU/mL. The suspension was further diluted in Mueller Hinton Broth (MHB, Biokar Diagnostics) to obtain 10^6 CFU/mL. A series of final concentrations of Ag-NPs, between 4096 and 16 μg/mL, were prepared using a 1:2 dilution factor. In addition, 100 μl of bacterial suspension was introduced at each concentration. The plates were incubated with agitation for 24 hours at 37°C. Next, 10 μl of 20 mg/mL 2,3–5 triphenyl tetrazolium chloride (TTC, Acros Organics, USA) solution was added to each well of the microtiter plate. The plates containing TTC were then incubated for 30 minutes at room temperature, and any change from colorless TTC to pink-red formazon indicates microorganism growth. Afterwards, plates were analyzed to evaluate bacterial growth in each well and determine MIC of Ag-NPs, which is the weakest concentration where no significant bacterial growth was observed.

After the determination of the MIC, TSA plates were inoculated with 10 μl of each well that did not exhibit a color change, and the plates were then incubated at 37 °C for 24 hours. The minimum concentration at which the inoculum's viability was reduced by 100 % was identified as the MBC.

2.6. Biofilm formation ability

Biofilm formation was assessed following the approach detailed by [34] with a few modifications. Briefly, A bacterial suspension (~1.50 ×10^8 CFU/mL) was prepared as described earlier and subsequently diluted to produce a suspension of around 10^6 CFU/mL. Each well of microplates was inoculated with 200 μl of the bacterial suspension. Control wells consisted of 200 μl of sterile TSB in place of bacteria. All tests were repeated in triplicate. After incubation at 37°C for 24 hours, non-adherent cells were thoroughly eliminated. The wells were carefully washed three times and oven-dried at 60° C for 45 minutes. The biofilms formed on the surface of the wells were then stained with 0.10 % crystal violet solution (200 μl per well) for 10–15 minutes. After staining, the wells were rinsed again 3–6 times to remove excess stain. To quantify biofilm formation, the crystal violet staining the biofilm was dissolved in 200 μl of ethanol solution in each well. After 10 minutes, the solution was moved to a new microplate, and its optical density at 570 nm was measured with a microplate ELISA reader (Thermo Scientific Multiskan, USA). The obtained OD values were compared with the predetermined cut-off value using Eq. 2 [35].

$$\text{ODcut-off} = \text{Average OD of the negative control} + (3 \times \text{standard deviation (SD) of Ods of negative control}) \quad (2)$$

To interpret the results, the strains can be classified into the following classes: Negative biofilm production, Weak biofilm production, Moderate biofilm production and Strong biofilm production (Table 1), according to the OD values calculated above.

Table 1
Classification of biofilm-forming ability [35].

Biofilms formation capacity	Cut-off value calculation
Negative	$OD \leq ODcut\text{-}off$
Weak	$ODcut\text{-}off < OD \leq 2 \times ODcut\text{-}off$
Moderate	$2 \times ODcut\text{-}off < OD \leq 4 \times ODcut\text{-}off$
Strong	$OD > 4 \times ODcut\text{-}off$

2.7. Antibiofilm activity of silver nanoparticles

Antibiofilm effect of silver nanoparticles was assessed through wells treatment before (biofilm inhibition) and after (biofilm eradication) biofilm formation using different concentrations of Ag-NPs.

2.7.1. Biofilm inhibition

Biofilm inhibition was evaluated using the approach outlined by [36] with some modification. A range of Ag-NPs concentrations was prepared, including MIC, MIC/2, MIC/4 and MIC/8, by mixing Ag-NPs with TSB medium to obtain the specified concentration. Afterward, 100 μl of each prepared Ag-NPs concentration was added to each well. Subsequently, an equivalent volume (100 μl) of the bacterial suspension (~10^6 CFU/mL) was added to the different Ag-NPs concentrations, giving a final volume of 200 μl per well. For the Biofilm formation control, the bacterial suspension was combined with TSB medium only. All tests were repeated in triplicate. The plates were left to incubate at 37°C for 24 hours without agitation. Then, they were washed three to six times to eliminate unattached cells.

2.7.2. Biofilm eradication

In the biofilm eradication assay, preformed biofilms were first developed according to Elsaid et al., 2023. as described in the "Biofilm formation" section [34].

The contents of each well were removed after incubation. To eliminate unattached cells, the wells were rinsed three to six times, then refilled with 200 μl of Ag-NPs at MIC, MIC/2, MIC/4 and MIC/8 concentrations. The untreated control consisted of a 200 μL solution of sterile physiological water alone. All tests were repeated in triplicate. Following this, the microplates were again incubated under biofilm-maintaining conditions, usually at room temperature, for 24 hours. After incubation, the Ag-NPs solution was then withdrawn and the wells were washed.

For both biofilm inhibition and eradication, the plates were dried at 60°C for 30 minutes. After this, the wells were then stained with 0.10 % crystal violet solution (200 μl per well) for 10–15 minutes and washed 3–6 times to remove excess colorant. The crystal violet associated with the biofilm was solubilized by adding 200 μl of ethanol solution to each well, and the contents of the wells were transferred to a new microplate for measurement of OD at 570 nm with a microplate ELISA reader (Thermo Scientific Multiskan). After determining mean absorbance of the samples, the percentage of biofilm inhibition and eradication was estimated using the following equation [37]:

$$\text{Percentage of inhibition or eradication} = (\text{OD Negative control-OD Experimental})/\text{OD Negative control} \times 100 \quad (3)$$

2.8. Statistical analysis

All tests were carried out in three replicates. A one-way ANOVA was conducted to assess the antibacterial activity of Ag-NPs against various bacterial strains at different concentrations. A two-way ANOVA with interaction factors was conducted to assess the biofilm inhibition and eradication effects of Ag-NPs against various bacterial strains at different concentrations. The ANOVA test employed was parametric, following an affirmative assessment of data normality (via normality plot of residuals and Shapiro-Wilk test) and equality of variances (via residuals versus fits plot and Levene's test). Data transformation using the natural logarithm transformation ($\ln(x + 1)$) was applied to improve normality. Subsequently, homogeneous groups were determined through pairwise multiple comparisons using the TukeyHSD function. Statistical analyses were performed using R-4.2.1 [64].

3. Results

3.1. Visual observation of Ag-NPs synthesis

Aqueous extract of *L. mairei* efficiently reduced silver ions to Ag-NPs, as indicated by the shift in mixture color from colorless to dark brown (Figs. 1–2). However, the silver nitrate solution incubated under the same conditions without the *L. mairei* extract did not exhibit any color change, as illustrated in Figs. 1–1.

3.2. UV–Vis spectral analysis

UV-Vis spectral analysis validated the biological synthesis of Ag-NPs. The analysis showed a strong absorption peak at around 440 nm (Fig. 2), demonstrating the effective production of silver nanoparticles. The intensity and position of the absorption peak were influenced by the various synthesis parameters, underscoring the need of optimizing these conditions to get a better understanding of their impact on Ag-NPs production.

3.3. Optimization of green synthesis of Ag-NPs

3.3.1. Influence of aqueous extract volume on the silver nanoparticles synthesis

Among the different volumes evaluated, a strong influence was revealed as shown in Fig. 3. In particular, the 0.50 mL volume showed the best synthesis results, with an intense absorption peak in the UV-Vis spectral analysis. Furthermore, a reduction in peak intensity was observed as the volume of the extract increased. Thus, it was determined that the optimum volume for Ag-NPs synthesis is 0.50 mL. This finding highlights the need for particular attention when choosing the extract volume for Ag-NPs synthesis, as higher volumes correlate with lower peak intensity, which has a negative effect on the synthesis process.

3.3.2. Influence of silver nitrate concentration on silver nanoparticles synthesis

The effect of silver nitrate concentration was examined with the aim of optimizing Ag-NPs synthesis. It was found in Fig. 4 that 1 mM was the ideal concentration for efficient Ag-NPs production. The UV-Vis absorption spectra revealed a significant absorption peak at this concentration. Importantly, as the silver nitrate concentration decreased below this optimal value, a reduction in the intensity of these absorption peaks was noted

3.3.3. Influence of reaction temperature on silver nanoparticles synthesis

Analysis of the UV–vis absorption spectra in Fig. 5 indicated that the reaction temperature of 70°C was the most appropriate of the temperatures tested. It was also observed that a lower temperature was accompanied by a corresponding reduction in the absorption spectrum. This suggests that lower temperatures could not be adequate for optimum absorption, affecting the synthesis process. These results underline the critical necessity of precisely controlling the reaction temperature in order to assure perfect synthesis of silver nanoparticles.

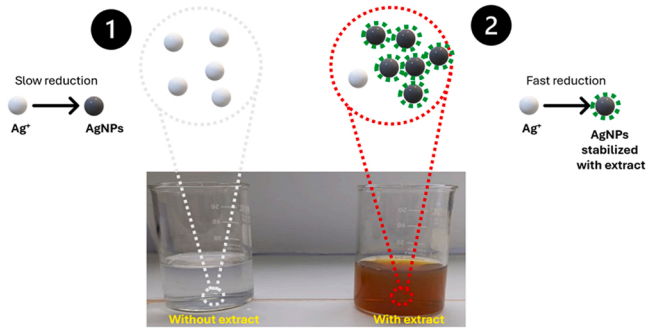

Fig. 1. Visible observation of (1) 1 mM silver nitrate solution and (2) Ag-NPs biosynthesis by aqueous extract of *L. mairei*.

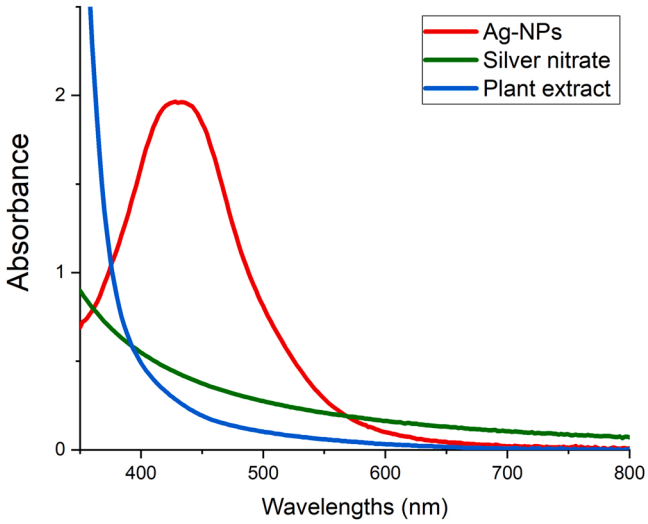

Fig. 2. UV–vis spectra of Ag-NPs biosynthesized from *L. mairei* aqueous extract, silver nitrate alone and plant extract alone.

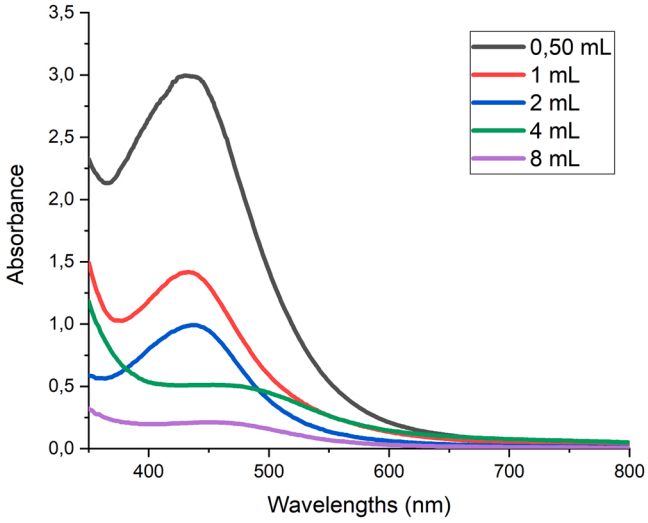

Fig. 3. UV–vis spectra of the effect of aqueous extract volume on Ag-NPs synthesis.

3.3.4. Influence of reaction time on silver nanoparticles synthesis

A study of the influence of reaction time on the biosynthesis of silver nanoparticles revealed that a reaction time of 2 hours was identified as sufficient for successful Ag-NP synthesis (Fig. 6). The selected reaction time of 2 hours produced a pointed and intense absorption peak in the UV-Vis spectral analysis. In contrast, the other reaction times, while producing exceptionally intense absorption peaks, lacked the pointed, well-defined character observed at 2 hours. These broader peaks indicate perhaps a larger nanoparticle size compared with the pointed-peak Ag-NPs obtained with the 2-hour reaction time. This implies the need for microscopic observation to explain this difference in absorption peaks.

3.4. Scanning electron microscopy

SEM analysis was employed for characterization of size and morphological of the synthesized silver nanoparticles. Fig. 7a–d shows

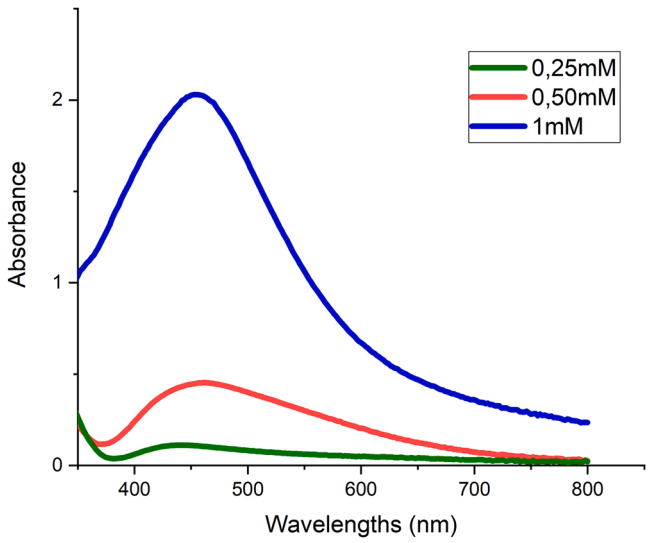

Fig. 4. UV–vis spectra of the effect of silver nitrate concentration on Ag-NPs synthesis.

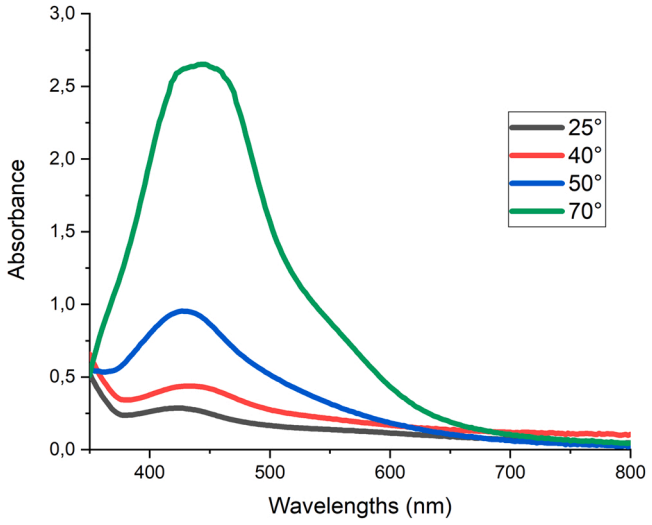

Fig. 5. UV–vis spectra of the effect of reaction temperature on Ag-NPs synthesis.

the findings, which provide light on how the properties of nanoparticles changed during the synthesis process

In Fig. 7a, which corresponds to a synthesis duration of 2 hours, the SEM images reveal silver nanoparticles with a consistently spherical morphology. The particles exhibit a well-defined and uniform shape, and their typical size is ranging between 30–60 nm. As the reaction time progresses, there is a noticeable increase in particle size. Specifically, Fig. 7b (4 hours) and Fig. 7c (6 hours), show a slight size increase, while Fig. 7d (8 hours) reveals more substantial growth beyond the initial range. Interestingly, the change in shape becomes more apparent as the response time increases. In contrast to the more heterogeneous structures shown in Fig. 7b, c, the 2 hours synthesis (Fig. 7a) retains an essentially spherical form.

3.5. Energy dispersive X-ray spectroscopy analysis

To assess the purity and composition of the sample in terms of its elemental constituents, EDS elemental analysis was conducted, as depicted in Fig. 8a. The resulting spectrum revealed distinct peaks corresponding to various elements. In particular, a strong peak at 3 keV

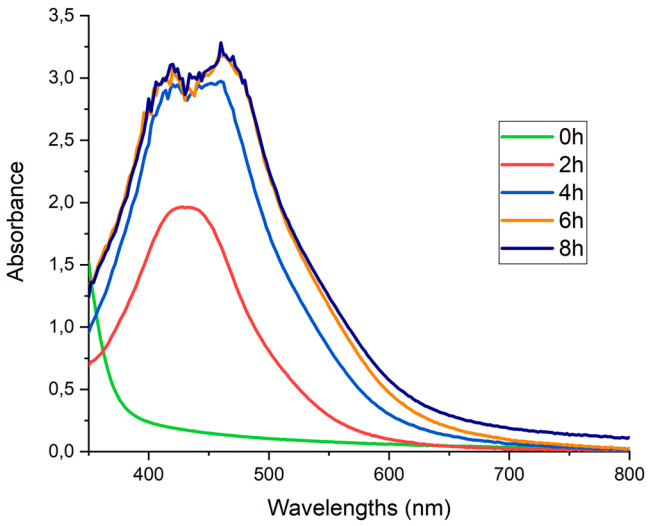

Fig. 6. UV–vis spectra of the effect of reaction time on Ag-NPs synthesis.

was identified, attributed to silver. Subsequently, the atomic percentages of each detected element were determined, and these results are illustrated in Fig. 8b. Specifically, the elemental composition indicated the presence of Carbon (C) at 16.20 %, Oxygen (O) at 4.83 %, Chlorine (Cl) at 6.67 %, and a predominant amount of Silver (Ag) at 72.30 %.

3.6. X-ray diffraction

The crystallinity of Ag-NPs biosynthesized from *L. marei* aqueous extract was confirmed through X-ray diffraction. Fig. 9 displays the diffraction pattern of Ag-NPs at 2θ values of 38.18°, 44.38°, 64.57°, 77.55° and 81.71° across the entire spectrum of the 2 Theta range from 10° to 100°, indicated by reflections (111), (200), (220), (311) and (222) of metallic silver. Moreover, Eq. (1) provided the mean crystal size of the biosynthesized silver nanoparticles, which was 11,328 ± 4505 nm.

3.7. Fourier Transform Infrared Spectroscopy Analysis (FTIR)

Infrared spectroscopy was used to examine the chemical composition of *L. mairei* extract and green synthesized Ag-NPs. The goal of this analysis was to identify potential biomolecules contributing to the creation of a protective layer, acting as a cap on the surface of the silver nanoparticles. The IR spectrum of *L. mairei* aqueous extract and silver nanoparticles exhibits common peaks at around 3208.95, 2355.13, 1529, 1370, 1260, 1040.78, and 697.94 cm^{-1}, and all these peaks are shown in Fig. 10.

3.8. Dynamic light scattering (DLS) analysis

Analysis of particle size using DLS revealed the presence of two peaks. One, displaying low intensity, was centered around 25.10 nm, while the other, with higher intensity, was centered around 124.47 nm (Fig. 11).

3.9. Antibacterial activity of silver nanoparticles

The results revealed that the Ag-NPs biosynthesized from the aqueous extract of *L. mairei* exhibited considerable efficiency against Acinetobacter strains as shown by the MICs presented in Table 2. The *A. baumannii* 1, *A. baumannii* 2, and *A. baumannii* 4 exhibited the highest antibacterial activity, with a MIC of 64 μg/mL. In contrast, the other *A. baumannii* strains needed a slightly higher concentration (MIC = 128 μg/mL) to be inhibited. Statistical analysis revealed highly significant differences ($P < 0.001$) among all the tested bacteria. Furthermore,

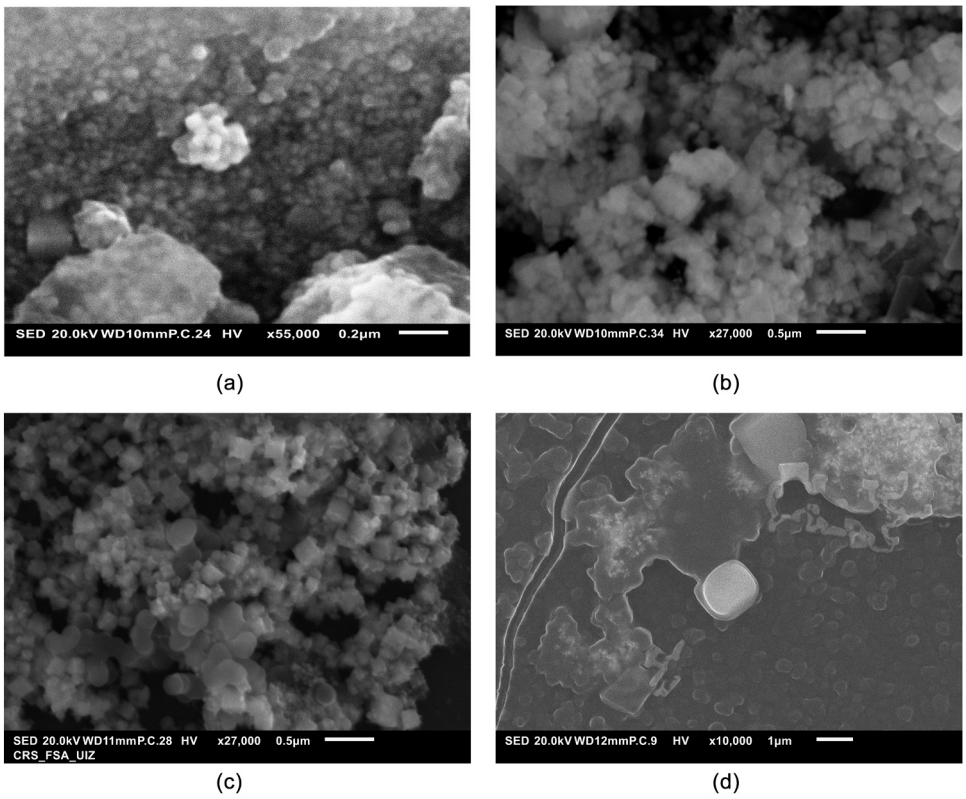

Fig. 7. SEM images of the biosynthesized Ag-NPs using *L. mairei* at different incubation times: 2 hours (a), 4 hours (b), 6 hours (c), and 8 hours (d).

it was shown that certain Acinetobacter strains needed to be in presence of concentrations above 512 µg/mL of Ag-NPs to exert bactericidal activity. On the other hand, some strains exhibited an MBC of 512 µg/mL, while others demonstrated MBC values of 256, 128 and 64 µg/mL (Table 2).

In addition to the efficacy against Acinetobacter strains, Ag-NP were also evaluated for their antibacterial activity against MDR Enterobacteriaceae species. The findings, detailed in Table 3, showed that strains 2, 4 and 9 of *K. pneumoniae* along, with strains 2 and 3 of *E. coli* had a MIC value of 128 µg/mL. In addition, the MIC values for *E. hormaechei* and *E. cloacae* were 256 µg/mL. Moreover, the MBC value for *E. coli* 2, *K. pneumoniae* 2, and *K. pneumoniae* 9 was determined to be 128 µg/mL, whereas, *E. coli* 3 and *E. cloacae* exhibited an MBC of 256 µg/mL. Furthermore, *E. hormaechei* and *K. pneumoniae* 4 displayed an MBC of 512 µg/mL. There is a significant difference among the tested strains (p value < 0.001).

3.10. Biofilm formation

The ability of the strains tested to form a biofilm on the titration microplates was assessed and the results are illustrated in Fig. 12. Incubation of bacterial suspensions for 24 hours revealed that ten (58.82 %) strains were strong biofilm producers with OD values above 0.36, three (17.64 %) strains were moderate biofilm producers with OD values between 0.18 and 0.36, and four (23.52 %) strains were weak biofilm producers (OD < 0.18). The strong and moderate biofilm-producing strains were selected for antibiofilm activity testing.

3.11. Antibiofilm activity of silver nanoparticles

3.11.1. Biofilm inhibition

The inhibitory effect of silver nanoparticles was tested on thirteen strains (Fig. 13). Results were expressed as biofilm inhibition percentages with the interaction effect strain-concentration demonstrating a very highly significant difference (p value < 0.001). Ag-NPs demonstrated a marked dose-dependent inhibitory effect on biofilm formation for al tested strains, except for *E. hormaechei* and *K. pneumoniae* 9 which was dose-independent. At MICs, the percentage of inhibition ranged from 40.50 ± 1.77 % to 95.22 ± 4.18 %. Among the strains, *A. baumannii* 1 proved to be the most susceptible to Ag-NPs at this concentration. Furthermore, when the Ag-NP concentration was reduced to MIC/2, inhibition percentages ranged from 36.33 ± 0.89 % to 80.07 ± 1.31 %, with *A. baumannii* 5 being the most sensitive among the strains. Additionally, Ag-NPs at MIC/4 exhibited inhibitory rates vary between 3.39 ± 0.76 and 70.37 ± 2.30 %. Once again, *A. baumannii* 5 was found to be more sensitive than the other strains. Finally, the inhibition percentages of Ag-NPs, for MIC/8 varied from 2.01 ± 1.13 % to 34.92 ± 2.43 %, with *A. baumannii* 6 displaying the highest sensitivity among all strains.

3.11.2. Biofilm eradication

Biofilm eradication studies were performed to validate the capabilities of the green synthesized Ag-NPs to eliminate preformed biofilm. A total thirteen strains were used to verify their biofilm-eradication capacity by adding different concentration of Ag-NPs such as MIC, MIC/2, MIC/4 and MIC/8. The biofilm eradication percentages after 24 h of incubation, as shown in Fig. 14, showed significant different (p value < 0.001) and indicated an increasing eradication in Ag-NPs concentration-dependent manner for all tested strains. Moreover, the most sensitive bacterium to the Ag-NPs among the strains tested was *A. baumannii* 6, which showed an eradication percentage of 46.95 ± 1.54 %, at a very low concentration corresponding to MIC/8. On the other hand, *E. coli* 2 biofilm was the most resistant, requiring the highest concentration (MIC) to be eradicated by only 38.32 ± 1.09 %.

4. Discussion

Numerous researches have explored and validated the biosynthesis

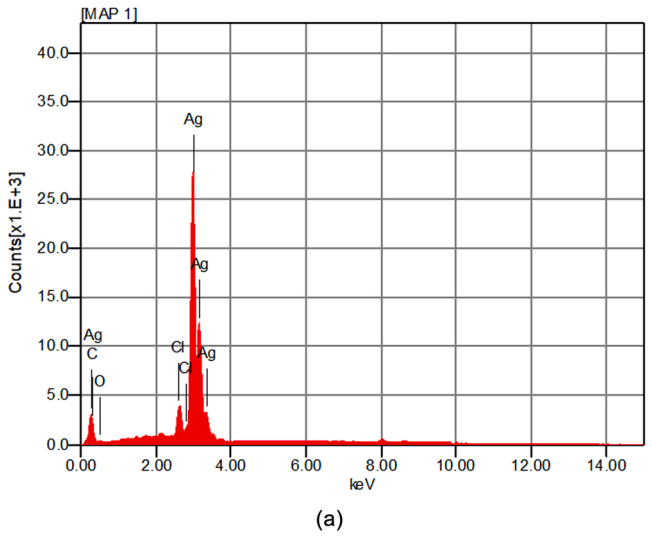

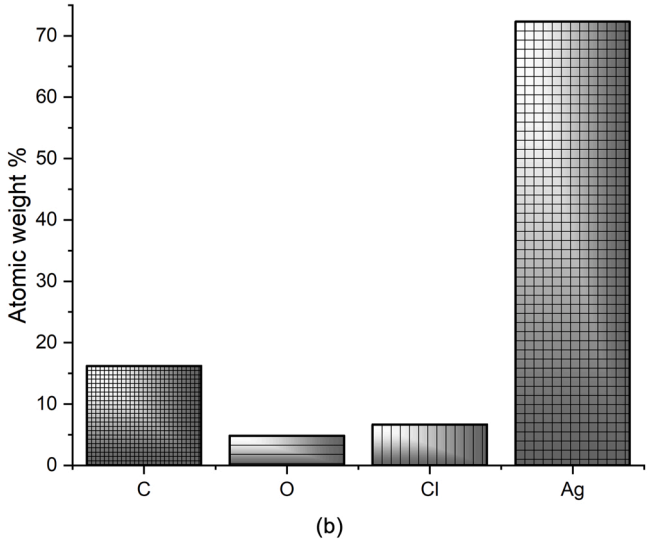

Fig. 8. EDS analysis of Ag-NPs synthesized by the aqueous extract of *L. mairei,* a) EDS.
spectrum of biosynthesized Ag-NPs; b) atomic percentage of atoms present in biologically.
synthesized Ag-NPs.

of nanoparticles as an effective antibacterial and antibiofilm agent [38, 39]. In this investigation, Ag-NPs were synthesized employing *L. mairei*. The marked shift in color from clear to dark brown, provides a visual indication of the success of silver nanoparticle production. This color change is due to the reduction of Ag^{+} ions to Ag^{0}, accompanied by the excitation of surface plasmon resonance (SPR) [40]. The biosynthesis of Ag-NPs was validated using UV–vis analysis, revealing a distinct peak at 440 nm. This peak is typical of spherical Ag-NPs and is attributable to the SPR band of Ag-NPs [41]. Specific synthesis conditions are a key factor in determining the efficiency of nanoparticle biosynthesis, as highlighted in the literature. Therefore, our study aims to systematically optimize key synthesis parameters, notably extract volume, $AgNO_3$ concentration, temperature, and reaction time, to minimize production costs and obtain nanoparticles of uniform size with well-defined morphology.

SEM stands out as a highly potent surface analysis technique, offering valuable insights into the composition, and topology of sample. This method proves exceptionally effective for scrutinizing the surface morphology of nanoparticles [39]. The production of Ag-NPs was

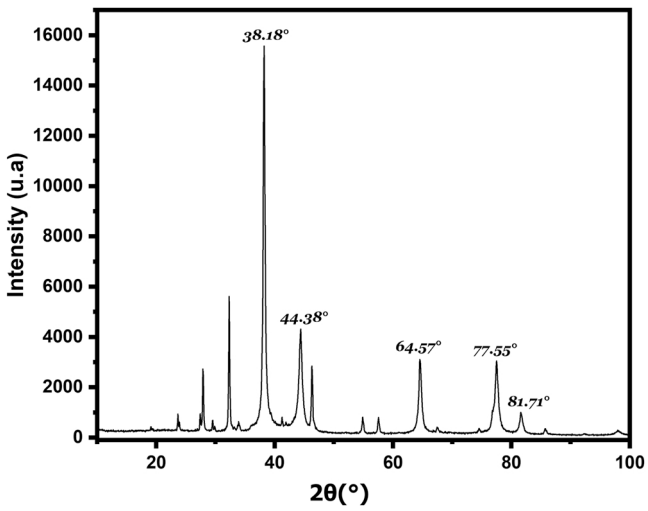

Fig. 9. X-ray diffraction pattern of Ag-NPs synthesized from *L. mairei*.

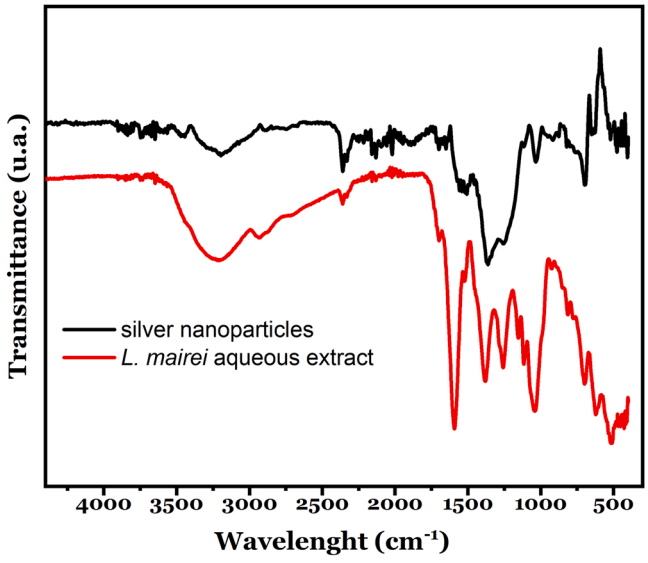

Fig. 10. FTIR spectrum of silver nanoparticles synthesized from *L. mairei*.

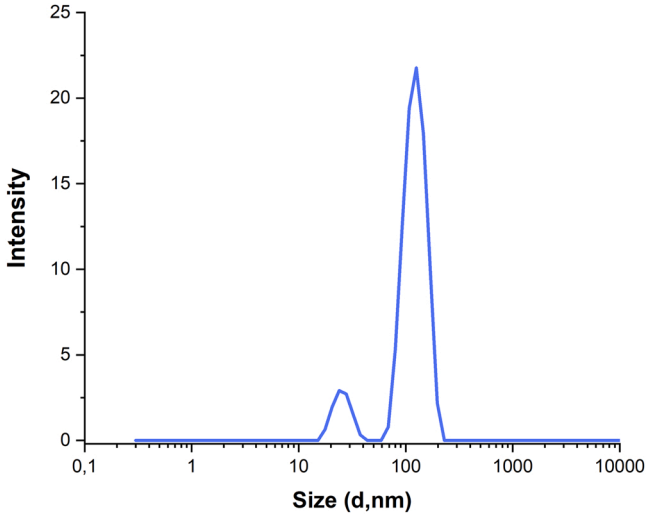

Fig. 11. Particle size distribution profile of biological silver nanoparticles.

Table 2
Antibacterial activity of Ag-NPs against Acinetobacter stains.

Pathogens	MIC (µg/mL)	MBC (µg/mL)
A. baumannii 1	64	> 512
A. baumannii 2	64	512
A. baumannii 3	128	256
A. baumannii 4	64	64
A. baumannii 5	128	> 512
A. baumannii 6	128	> 512
A. baumannii 8	128	128
A. baumannii 9	128	256
A. baumannii 10	128	512
A. baumannii 11	128	128

Table 3
Antibacterial efficacy of Ag-NPs against Enterobacteriaceae species.

Pathogens	MIC (µg/mL)	MBC (µg/mL)
E. coli 2	128	128
E. coli 3	128	256
K. pneumoniae 2	128	128
K. pneumoniae 4	128	512
K. pneumoniae 9	128	128
E. cloacae	256	256
E. hormaechei	256	512

studied by MEB imaging. Four images were captured at various times to observe the evolution of the size and form of the nanoparticles. The results demonstrate that the properties of nanoparticles depend on the synthesis conditions. In particular, MEB images show that the nanoparticles formed at the initial stage of the synthesis process (after 2 hours incubation) are spherically approximately uniform and have a size range of 30–60 nm (Fig. 7.a). However, as the synthesis progresses, the size and morphology of the nanoparticles change, resulting in particles of a different shape and larger size than those biosynthesized in the early stages. These results indicate that synthetic conditions have an important role to play in determining the characteristics of nanoparticles, and optimizing these conditions can lead to the production of Ag-NPs with particular size and shapes. These findings are consistent with the results of a previous study, which showed that as reaction time increased, the mean diameters of Ag-NPs progressively increased [42]. The EDS profile of the biosynthesized Ag-NPs (Fig. 8.a) reveals the presence of a peak at 3 keV, which corresponds to the typical absorption of silver [43]. Additionally, as illustrated in Fig. 8.a, the biosynthesized silver nanoparticles are primarily composed of silver (72.30 %), with the remaining percentages attributed to carbon (16.20 %), oxygen (4.83 %), and chlorine (6.67 %). This indicates that the synthesis of nanoparticles was successful with an abundant amount of silver in the sample, providing valuable insights into the high purity of these silver nanoparticles biosynthesis. Similar findings were obtained by Qais et al. [28] who reported that the elemental composition of their biosynthesized Ag-NPs was 60.86 % silver, 19.84 % carbon, 12.53 % oxygen and 6.77 % chlorine by weight [28].

XRD is one of the techniques commonly employed to determine parameters like the crystal size of materials in powder or thin film form [44]. During the XRD measurement analysis, X-rays are aimed at the sample specimen and subsequently interact with the electron clouds of atoms within the sample. A detector is employed to gauge the X-ray intensity while varying the angle of beam diffraction [45]. In this study, the XRD pattern of nanoparticles displayed prominent peaks in the 2θ range from 10° to 100°. Indeed, Ag-NPs, synthesized from *L. mairei*, exhibited distinct XRD peaks with 2θ values at 38.18°, 44.38°, 64.57°, 77.55° and 81.71°, corresponding to the characteristic peaks of face-centered cubic silver, as referenced in the Open Crystallography Database with number of 9011607. Previous studies have also reported comparable patterns for the Ag-NPs [43,46]. The mean size of the silver nanoparticles, determined using the Debye-Scherrer formula, was found

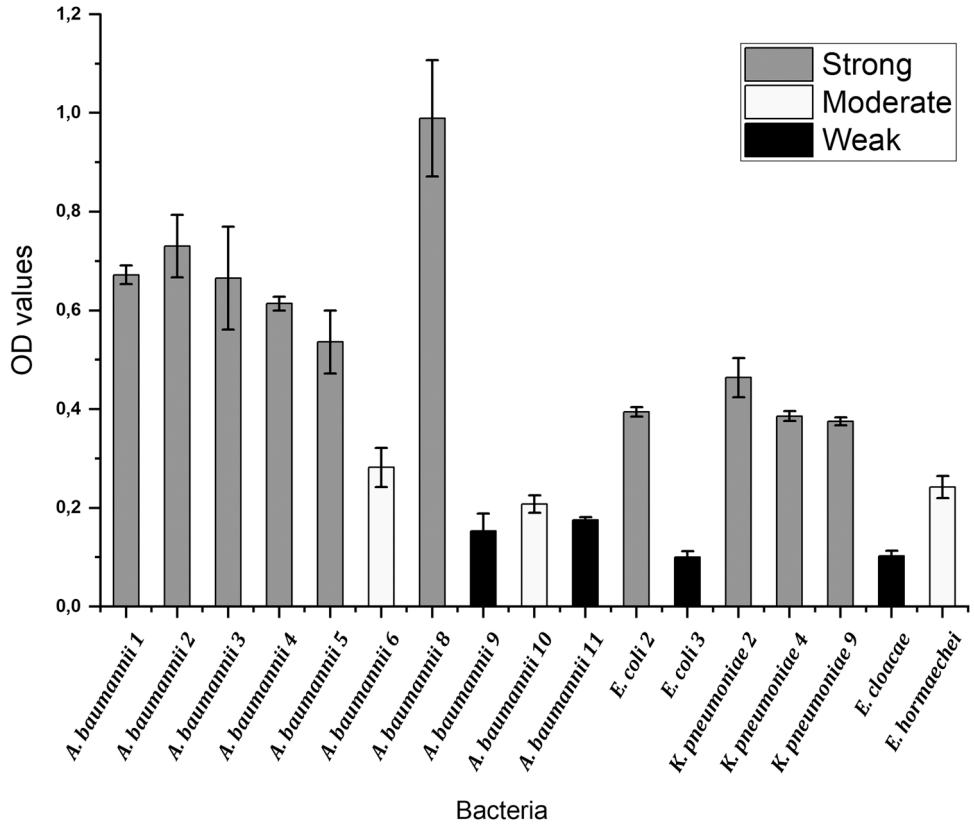

Fig. 12. Optical Density (OD) and biofilm formation capacity of MDR *A. baumannii* strains and Enterobacteriaceae species after 24 hours of incubation.

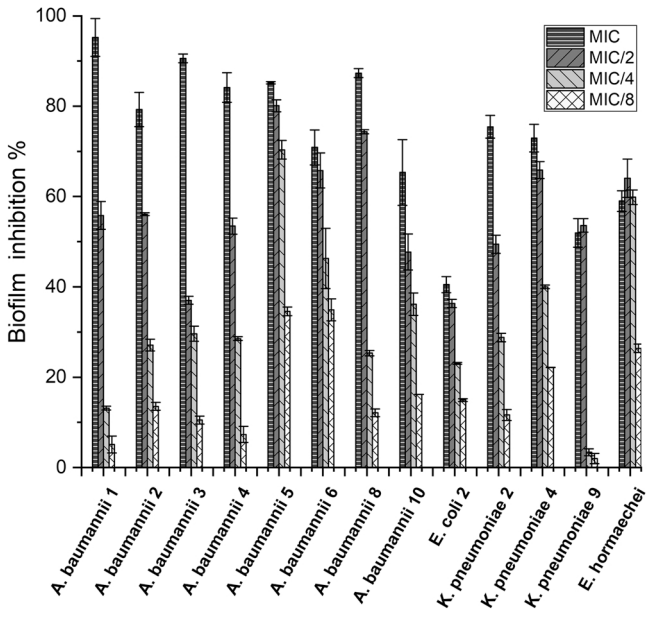

Fig. 13. Inhibition of biofilm formation by Ag-NPs against *A. baumannii* and Enterobacteriaceae strains.

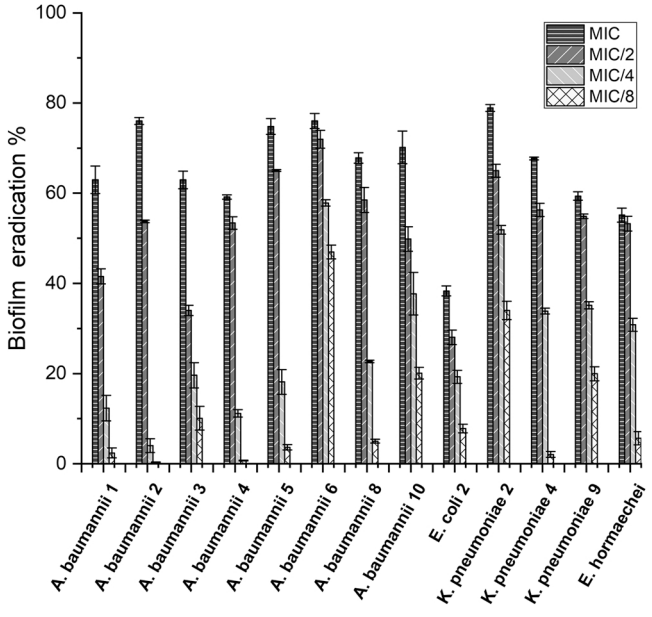

Fig. 14. Biofilm eradication activity of Ag- NPs against *A. baumannii* and Enterobacteriaceae strains.

to be 11,32 ± 4,50 nm, strongly in line with average size of approximately 12.10 nm reported by Sun et al. [47].

FT-IR stands out as an extensively utilized technique for qualitatively characterizing diverse molecules, determining the molecular structure of provided substances, and identifying functional groups within a molecular structure. Its principle lies in atoms' vibrational response to infrared radiation, gauging absorption quantities and qualities of emitted radiation in the sample [48]. The FTIR spectrum revealed distinct peaks demonstrating the existence of diverse functional groups in both *L. mairei* aqueous extract and the synthesized nanoparticles, suggesting their persistence after the synthesis process. A broad peak in 3208.95 cm^{-1} suggests the existence of O-H or H-bonded bands found in phenolic or alcoholic compounds [49]. The peak observed at 2355.13 cm^{-1} may arise from the stretching vibrations of C═O in proteins and carboxylic compounds [40]. Additionally, the observed peak at 1529 cm^{-1} represents the N–H bond found in amides, while the peaks at 1370 cm^{-1} indicated the existence of CH_3-CH bonds in alkanes and alkyl groups [28], and the peaks found at 1260 cm^{-1} and 1040.78 cm^{-1} can be attributed to C-O bonds in carboxylic acids, alcohols ester and ethers covalently bound to nanoparticles [48]. Furthermore, the peak at 697.94 cm^{-1} was associated with C-H bonding in aromatic compounds [28]. In addition to their stabilizing role, the presence of these functional groups in biosynthesized nanoparticles can reduce aggregation and simultaneously act as reducing agents [41].

Particle size analysis by DLS revealed two distinct peaks, with values centered around 25.10 nm and 124.47 nm. The particle sizes measured by XRD were found to be much smaller than those found by DLS analysis. This discrepancy may be due to the fact that XRD measures only the size distribution based on physical parameters, not accounting for any capping agent. In contrast, a particle-size analyzer determines the hydrodynamic diameter, including the particle size of molecules or ions attached to the surface, leading to larger measurements compared to XRD [50].

The antibacterial effectiveness was assessed using the microdilution technique with different concentrations of Ag-NPs. This test reveals the MBC and MIC against various MDR strains. As detailed in Tables 2 and 3, the selected strains, including *A. baumannii, E. hormaechei, E. coli, K. pneumoniae*, and *E. cloacae*, demonstrated significant sensitivity to the Ag-NPs synthesized through green methods. The MIC values, between from 64 and 256 μg/mL, further underscore the substantial and promising antibacterial activity exhibited by the Ag-NPs synthesized with *L. mairei* aqueous extract against the tested strains. In a comparable study, the antibacterial property of Ag-NPs was tested against *A. baumannii, E. coli*, and *K. pneumoniae*, revealing an inhibitory concentration of 250 μg/mL [38]. Furthermore, a study found that silver nanoparticles biosynthesized from *Senna alata* bark extract exhibited notable antibacterial efficacy against *A. baumannii*. The MIC and MBC values were determined to be 62.50 and 250 μg/mL, respectively. The researchers hypothesized that these nanoparticles could potentially interact with DNA, transporter proteins, and intracellular enzymes, inducing cell damage. Additionally, they suggested that silver ions could bind with DNA, leading to its fragmentation [51]. Moreover, Avirdi et al., 2023. highlighted that the antibacterial efficacy of Ag-NPs against *E. cloacae* was observed at 250 μg/mL, demonstrating a comparable result to the biosynthesized silver nanoparticles in our study (MIC of 256 μg/mL) [52]. It is crucial to emphasize that the elevated effectiveness of nanoparticles typically associated with their small size, as smaller particles are able to interact rapidly and readily with the cell surface penetrate the cytoplasm due to a lower spatial barrier [53].

The majority of bacterial species prefer to live in biofilm communities instead of planktonic cells. Indeed, the biofilms formation is a crucial element in the pathogenicity of bacteria, enabling them to evade the human immune system and resist to the effects of antibiotics [53]. They are often at the root of chronic nosocomial infections in clinical environments. The formation of biofilm not only shields bacteria from the effect of antibiotic, but also promotes the spread of infections. Additionally, biofilm development is a significant issue in clinical settings where medical devices like urine catheters and hemodialysis machines are used. Around 70 % of cases of bacterial infection result from biofilm, whether or not they are related to medical devices [54]. Therefore, this research evaluated the formation of biofilms by various bacterial strains of *A. baumannii* and Enterobacteriaceae was evaluated. The results indicate that 58.82 % of the strains exhibited strong biofilm production, 17.64 % displayed moderate biofilm production, while 23.52 % demonstrated weak biofilm production. This observation suggests that, for strains with weak biofilm, the 24 hours incubation time might be insufficient to allow the formation of a strong biofilm [11]. Additionally, the medium culture and the support can also lead to the formation of smaller biofilms compared to in situ biofilms. In another study by Yang et al., 15.60 % of the bacterial strains evaluated were

found to be weak biofilm producer, whereas 32.50 % and 45.40 % were capable to form moderate or strong biofilms, respectively [55].

Developing new strategies to combat the major risk caused by Biofilm-associated MDR bacteria is vital. [56]. The antibiofilm activity of Ag-NPs showed varied effects against the diverse tested microorganisms. Indeed, these silver nanoparticles exhibited a considerable effect against biofilm formation and eradication of all tested strains, with inhibition and eradication percentage varying according to bacteria and concentration. These variations in antibiofilm activity could result from variations in biofilm structure and composition between the different strains examined [53]. In agreement with our findings, Mohanta et al., revealed a remarkable antibiofilm activity of plant-produced Ag-NPs against the human pathogen *E. coli* [39]. Moreover, Barabadi et al., reported that *Penicillium chrysogenum*-Derived Ag-NPs at MIC/2 exhibited greater potency in inhibiting biofilm formation of pathogenic *A. baumannii* than did tetracycline [57]. Furthermore, Singh et al., showed that biological Ag-NPs effectively eradicated the preformed biofilm of *A. baumannii* AIIMS 7. Furthermore, the eradication of mature biofilm was enhanced by their exposure to Ag-NPs in combination with the antibiotics [58]. In another study, Xia et al., reported that at concentration of 60 μg/mL, the biofilm inhibition rate of the biosynthesized Ag-NPs on strong biofilm-forming XDR-*K. pneumoniae* strains was higher than 80 % [59]. The observed biofilm inhibition and eradication at concentrations below the MIC value could be attributed to non-lethal damage or to inhibition of gene expression involved in motility and formation of biofilm [60]. Furthermore, Mohanta et al., suggested that antibiofilm action of Ag-NPs might be due to inhibition of bacterial EPS production, which is a necessary step in the formation of biofilms [39]. It should be also noted that the anti-biofilm activities can be attributed to the functions of the Ag^{+} ions released by the silver nanoparticles, which are adsorbed onto the surface of bacterial cells and injure cells by modifying the properties of enzymes and structure of proteins [61]. In addition, our findings also showed that the elimination of preformed biofilm needed a higher concentration than the biofilm inhibition concentration for most of the tested bacteria. This observation is valid for all bacteria, with the exception of *A. baumannii* 6, and 10 and the three strains of *K. pneumoniae*. These findings are similar to those previously reported by Toranzo et al. in their study of *Yersinia enterocolitica*. [53]. Mature biofilms have a complex structure which renders them more resistant. The extracellular matrix encasing the biofilm functions as a protective barrier, which means that higher concentrations may be required to penetrate and eradicate the preformed biofilm [62]. Additionally, previous research has shown that when bacteria are subjected to extreme conditions, such as being exposed to antibiofilm agents, they are more inclined to exist in a planktonic state [63]. This phenomenon explains the high efficacy of these green synthesized Ag-NPs in inhibiting the formation of biofilms.

5. Conclusion

MDR bacteria represent a significant and growing threat to public health worldwide, owing largely for their resistance to antibiotics and their capacity to form long-lasting biofilms. This study highlights, for the first time, the potential of *L. mairei*-mediated silver nanoparticles as an effective strategy against biofilm-forming multidrug-resistant bacteria. The optimized synthesis parameters allowed the production of highly stable and uniform nanoparticles, which exhibited strong antibiofilm activity against *A. baumannii* and Enterobacteriaceae. Indeed, further research is needed to understand the mechanisms behind the antimicrobial and antibiofilm action of these Ag-NPs. Furthermore, understanding how they interact with bacterial cells and disrupt biofilm formation will help to better define their therapeutic action and accelerate their adoption in clinical practice, thus contributing to the global fight against antimicrobial resistance. These findings hold significant translational potential, as the Ag-NPs could, after further testing (e.g. biocompatibility, toxicity, in vivo antimicrobial activity among others), be integrated into wound dressings, medical device coatings, or topical antimicrobial formulations to combat MDR infections in hospital settings.

Funding

This work was supported by the Ministry of National Education, Vocational Training, Higher Education, and Scientific Research, the National Agency for Medicinal and Aromatic Plants, and the Moroccan National Center of Scientific and Technical Research (VPMA3; n°: 576/2021).

CRediT authorship contribution statement

Msanda Fouad: Resources. **Reffuveille Fany:** Writing – review & editing, Validation. **hamadi fatima:** Writing – review & editing, Writing – original draft, Visualization, Validation, Supervision, Software, Resources, Methodology, Formal analysis, Data curation, Conceptualization. **Hassi Mohamed:** Writing – review & editing, Visualization, Validation. **Diguță Camelia Filofteia:** Writing – review & editing, Validation, Resources. **Abou Oualid Hicham:** Validation, Methodology, Formal analysis. **Gangloff Sophie C:** Writing – review & editing, Validation. **Matei Florentina:** Writing – review & editing, Validation, Resources. **Elkheloui Raja:** Writing – review & editing, Validation. **Laktib Asma:** Writing – review & editing, Formal analysis. **EL Megdar Soufiane:** Writing – review & editing, Writing – original draft, Visualization, Validation, Software, Methodology, Formal analysis, Data curation, Conceptualization.

Declaration of Generative AI and AI-assisted technologies in the writing process

During the preparation of this work, the authors used ChatGPT-3.5 and DeepL to enhance language clarity and readability. After employing these tools, the authors thoroughly reviewed and edited the content as needed, taking full responsibility for the content of final publication.

Declaration of Competing Interest

The authors declare that they have no known competing financial interests or personal relationships that could have appeared to influence the work reported in this paper.

Acknowledgements

We gratefully acknowledge Kamel SHOUEIR for his invaluable assistance with revising this manuscript. We also thank Ilyass FILALI ALAOUI for his expertise in statistical analysis and Elmostafa HAMADI for English correction. Their contributions have significantly enhanced the quality of this research.

Appendix A. Supporting information

Supplementary data associated with this article can be found in the online version at doi:10.1016/j.colsurfa.2025.136544.

Data Availability

No data was used for the research described in the article.

References

[1] M. Frieri, K. Kumar, A. Boutin, Antibiotic resistance, J. Infect. Public Health 10 (2017) 369–378, https://doi.org/10.1016/j.jiph.2016.08.007.
[2] S.K. Ahmed, S. Hussein, K. Qurbani, R.H. Ibrahim, A. Fareeq, K.A. Mahmood, M. G. Mohamed, Antimicrobial resistance: Impacts, challenges, and future prospects,

J. Med. Surg. Public Health 2 (2024) 100081, https://doi.org/10.1016/j.glmedi.2024.100081.
[3] M. Naghavi, S.E. Vollset, K.S. Ikuta, L.R. Swetschinski, T. Mestrovic, G. Smith, C. Han, Global burden of bacterial antimicrobial resistance 1990–2021: a systematic analysis with forecasts to 2050, Lancet 404 (2024) 1199–1226, https://doi.org/10.1016/S0140-6736(24)01867-1.
[4] J. Lawrence, D. O'Hare, J. van Batenburg-Sherwood, M. Sutton, A. Holmes, T. M. Rawson, Innovative approaches in phenotypic beta-lactamase detection for personalised infection management, Nat. Commun. 15 (2024) 9070, https://doi.org/10.1038/s41467-024-53192-7.
[5] WHO bacterial priority pathogens list, 2024: Bacterial pathogens of public health importance to guide research, development and strategies to prevent and control antimicrobial resistance, (n.d.). ⟨https://www.who.int/publications/i/item/9789240093461⟩ (accessed January 30, 2025).
[6] A. Gedefie, E. Alemayehu, O. Mohammed, G.M. Bambo, S.S. Kebede, B. Kebede, Prevalence of biofilm producing Acinetobacter baumannii clinical isolates: A systematic review and meta-analysis, PLoS ONE 18 (2023) e0287211, https://doi.org/10.1371/journal.pone.0287211.
[7] N. Høiby, O. Ciofu, H.K. Johansen, Z. Song, C. Moser, P.Ø. Jensen, S. Molin, M. Givskov, T. Tolker-Nielsen, T. Bjarnsholt, The clinical impact of bacterial biofilms, Int. J. Oral. Sci. 3 (2011) 55–65, https://doi.org/10.4248/IJOS11026.
[8] Y. Liu, L. Wu, J. Han, P. Dong, X. Luo, Y. Zhang, L. Zhu, Inhibition of biofilm formation and related gene expression of listeria monocytogenes in response to four natural antimicrobial compounds and sodium hypochlorite, Front. Microbiol. 11 (2021), https://doi.org/10.3389/fmicb.2020.617473.
[9] J.A. Gaddy, A.P. Tomaras, L.A. Actis, The *Acinetobacter baumannii* 19606 OmpA protein plays a role in biofilm formation on abiotic surfaces and in the interaction of this pathogen with eukaryotic cells, Infect. Immun. 77 (2009) 3150–3160, https://doi.org/10.1128/IAI.00096-09.
[10] M. Maheshwari, I. Ahmad, A.S. Althubiani, Multidrug resistance and transferability of bla CTX-M among extended-spectrum β-lactamase-producing enteric bacteria in biofilm, J. Glob. Antimicrob. Resist. 6 (2016) 142–149, https://doi.org/10.1016/j.jgar.2016.04.009.
[11] M. Choudhary, R. Shrivastava, J. Vashistt, Acinetobacter baumannii Biofilm formation: association with antimicrobial resistance and prolonged survival under desiccation, Curr. Microbiol. 79 (2022) 361, https://doi.org/10.1007/s00284-022-03071-5.
[12] L. Surgers, A. Boyd, P.-M. Girard, G. Arlet, D. Decré, Biofilm formation by ESBL-producing strains of Escherichia coli and Klebsiella pneumoniae, Int. J. Med. Microbiol. 309 (2019) 13–18, https://doi.org/10.1016/j.ijmm.2018.10.008.
[13] SPF, Surveillance de l'antibiorésistance en établissement de santé. Données 2018. Partie 2: résistance bactérienne aux antibiotiques, (n.d.). ⟨https://www.santepubliquefrance.fr/import/surveillance-de-l-antibioresistance-en-etablissement-de-sante.-donnees-2018.-partie-2-resistance-bacterienne-aux-antibiotiques⟩ (accessed February 1, 2025).
[14] N. Faisal, K. Kumar, Polymer and metal nanocomposites in biomedical applications, Biointerface Res. Appl. Chem. 7 (2017) 2286–2294.
[15] A.-C. Burduşel, O. Gherasim, A.M. Grumezescu, L. Mogoantă, A. Ficai, E. Andronescu, Biomedical applications of silver nanoparticles: an up-to-date overview, Nanomaterials 8 (2018) 681, https://doi.org/10.3390/nano8090681.
[16] S.S. Salem, A mini review on green nanotechnology and its development in biological effects, Arch. Microbiol. 205 (2023) 128, https://doi.org/10.1007/s00203-023-03467-2.
[17] M. Fahim, A. Shahzaib, N. Nishat, A. Jahan, T.A. Bhat, A. Inam, Green synthesis of silver nanoparticles: a comprehensive review of methods, influencing factors, and applications, JCIS Open 16 (2024) 100125, https://doi.org/10.1016/j.jciso.2024.100125.
[18] N.S. Alsaiari, F.M. Alzahrani, A. Amari, H. Osman, H.N. Harharah, N. Elboughdiri, M.A. Tahoon, Plant and microbial approaches as green methods for the synthesis of nanomaterials: synthesis, applications, and future perspectives, Molecules 28 (2023) 463, https://doi.org/10.3390/molecules28010463.
[19] H.J. Nelagadarnahalli, G.K. Jacob, D. Prakash, R.R. Iska, V.B.R. Iska, F. Ameen, U. M. Rajadurai, N. Polachi, J.A. Jacob, Optimization and fabrication of silver nanoparticles to assess the beneficial biological effects besides the inhibition of pathogenic microbes and their biofilms, Inorg. Chem. Commun. 156 (2023) 111140, https://doi.org/10.1016/j.inoche.2023.111140.
[20] C. Vanlalveni, S. Lallianrawna, A. Biswas, M. Selvaraj, B. Changmai, S.L. Rokhum, Green synthesis of silver nanoparticles using plant extracts and their antimicrobial activities: a review of recent literature, RSC Adv. 11 (2021) 2804–2837, https://doi.org/10.1039/D0RA09941D.
[21] A. Laktib, K. Nayme, A.E. Hamdaoui, M. Timinouni, M. Hassi, A. Aitalla, F. Msanda, M. Bourouache, M.E. Yaagoubi, R. Mimoun, B. Bihadassen, F. Hamadi, Antibacterial activity of Lavandula mairei Humbert essential oil against carbapenem- resistant Acinetobacter baumannii, Mediterr. J. Infect. Microbes Antimicrob. 11 (2022), https://doi.org/10.4274/mjima.galenos.2021.2021.3.
[22] A. El Hamdaoui, F. Msanda, H. Boubaker, D. Leach, I. Bombarda, P. Vanloot, N. El Aouad, A. Abbad, E.H. Boudyach, F. Achemchem, A. Elmoslih, A. Ait Ben Aoumar, A. El Mousadik, Essential oil composition, antioxidant and antibacterial activities of wild and cultivated Lavandula mairei Humbert, Biochem. Syst. Ecol. 76 (2018) 1–7, https://doi.org/10.1016/j.bse.2017.11.004.
[23] A. El Hamdaoui, H. Mechqoq, M. El Yaagoubi, A. Bouglad, A. Hallouti, A. El Mousadik, N. El Aouad, A. Ait Ben Aoumar, F. Msanda, Effect of pretreatment, temperature, gibberellin (GA3), salt and water stress on germination of Lavandula mairei Humbert, J. Appl. Res. Med. Aromat. Plants 24 (2021) 100314, https://doi.org/10.1016/j.jarmap.2021.100314.
[24] M. Abouri, A.E. Mousadik, F. Msanda, H. Boubaker, B. Saadi, K. Cherifi, An ethnobotanical survey of medicinal plants used in the Tata Province, Morocco, Int J. Med Plants Res 1 (2012) 99–123.
[25] R. El Kheloui, A. Laktib, S. Elmegdar, L. Fayzi, C. Zanane, F. Msanda, K. Cherifi, H. Latrache, R. Mimouni, F. Hamadi, Anti-adhesion and antibiofilm activities of *Lavandula mairei* humbert essential oil against *Acinetobacter baumannii* isolated from hospital intensive care units, Biofouling 38 (2022) 953–964, https://doi.org/10.1080/08927014.2022.2149326.
[26] A. Laktib, M. Hassi, F. Hamadi, R. Mimouni, M. Bourouache, B. Bihadassen, A. A. Alla, Identification and antibiotic resistance of nosocomial bacteria isolated from the hospital environment of two intensive care units, Moroc. J. Biol. (2018) 28–41.
[27] A. Laktib, K. Nayme, L. Fayzi, R. El Kheloui, S. El Megdar, F. Msanda, M. Timinouni, K. Cherifi, M. Hassi, A. Ait Alla, R. Mimouni, F. Hamadi, Antibacterial and antibiofilm activities of *Thymus leptobotrys* and *Lavandula mairei* essential oils against extended spectrum β-lactamase producing *Enterobacteriaceae*, J. Essent. Oil Bear. Plants 27 (2024) 356–373, https://doi.org/10.1080/0972060X.2024.2325101.
[28] F.A. Qais, A. Shafiq, H.M. Khan, F.M. Husain, R.A. Khan, B. Alenazi, A. Alsalme, I. Ahmad, Antibacterial effect of silver nanoparticles synthesized using *Murraya koenigii* (L.) against multidrug-resistant pathogens, Bioinorg. Chem. Appl. 2019 (2019) e4649506, https://doi.org/10.1155/2019/4649506.
[29] M.K. Peiris, C.P. Gunasekara, P.M. Jayaweera, N.D. Arachchi, N. Fernando, Biosynthesized silver nanoparticles: are they effective antimicrobials? Mem. Inst. Oswaldo Cruz 112 (2017) 537–543, https://doi.org/10.1590/0074-02760170023.
[30] M. Cakić, S. Glišić, G. Nikolić, G.M. Nikolić, K. Cakić, M. Cvetinov, Synthesis, characterization and antimicrobial activity of dextran sulphate stabilized silver nanoparticles, J. Mol. Struct. 1110 (2016) 156–161, https://doi.org/10.1016/j.molstruc.2016.01.040.
[31] A. Pandey, K. Gupta, A. Pandey, Effect of nanosized TiO2 on photofermentation by Rhodobacter sphaeroides NMBL-02, Biomass-.-. Bioenergy 72 (2015) 273–279, https://doi.org/10.1016/j.biombioe.2014.10.021.
[32] F.A. Qais, A. Shafiq, I. Ahmad, F.M. Husain, R.A. Khan, I. Hassan, Green synthesis of silver nanoparticles using *Carum copticum*: Assessment of its quorum sensing and biofilm inhibitory potential against gram negative bacterial pathogens, Microb. Pathog. 144 (2020) 104172, https://doi.org/10.1016/j.micpath.2020.104172.
[33] M.M. Bazargani, J. Rohloff, Antibiofilm activity of essential oils and plant extracts against Staphylococcus aureus and Escherichia coli biofilms, Food Control 61 (2016) 156–164, https://doi.org/10.1016/j.foodcont.2015.09.036.
[34] E.M. Elsaid, O.I. Ahmed, A.M. Abdo, S.A. Abdel Salam, Antimicrobial and antibiofilm effect of silver nanoparticles on clinical isolates of multidrug resistant Klebsiella pneumoniae, Microbes Infect. Dis. 4 (2023) 542–554, https://doi.org/10.21608/mid.2023.200483.1487.
[35] A. Ghasemian, S. Najar Peerayeh, B. Bakhshi, M. Mirzaee, Comparison of biofilm formation between methicillin-resistant and methicillin-susceptible isolates of staphylococcus aureus, Iran, Biomed. J. 20 (2016) 175–181, https://doi.org/10.7508/ibj.2016.03.007.
[36] J. Ruiz-Duran, R. Torres, E.E. Stashenko, C. Ortiz, Antifungal and antibiofilm activity of colombian essential oils against different candida strains, Antibiotics 12 (2023) 668, https://doi.org/10.3390/antibiotics12040668.
[37] R. Srikanth, M.K. Thupurani, B. H.R, C. Surekha, Anti-biofilm activity and time kill kinetic effects of Salacia oblanga wall leaf and root extracts against clinical multi-drug resistance bacteria, Biomedicine 40 (2020) 347–352, https://doi.org/10.51248/.v40i3.24.
[38] M. Younas, M.H. Rasool, M. Khurshid, A. Khan, M.Z. Nawaz, I. Ahmad, M. N. Lakhan, Moringa oleifera leaf extract mediated green synthesis of silver nanoparticles and their antibacterial effect against selected gram-negative strains, Biochem. Syst. Ecol. 107 (2023) 104605, https://doi.org/10.1016/j.bse.2023.104605.
[39] Y.K. Mohanta, K. Biswas, S.K. Jena, A. Hashem, E.F. Abd_Allah, T.K. Mohanta, Anti-biofilm and antibacterial activities of silver nanoparticles synthesized by the reducing activity of phytoconstituents present in the Indian medicinal plants, Front. Microbiol. 11 (2020) 1143, https://doi.org/10.3389/fmicb.2020.01143.
[40] G.S. Reddy, K.V. Saritha, Y.M. Reddy, N.V. Reddy, Eco-friendly synthesis and evaluation of biological activity of silver nanoparticles from leaf extract of Indigofera barberi Gamble: an endemic plant of Seshachalam Biosphere Reserve, SN Appl. Sci. 1 (2019) 968, https://doi.org/10.1007/s42452-019-1008-0.
[41] Z. Haris, I. Ahmad, Green synthesis of silver nanoparticles using Moringa oleifera and its efficacy against gram-negative bacteria targeting quorum sensing and biofilms, J. Umm Al-Qura Univ. Appl. Sci. 10 (2023) 156–167, https://doi.org/10.1007/s43994-023-00089-8.
[42] S.K. Balavandy, K. Shameli, D.R.B.A. Biak, Z.Z. Abidin, Stirring time effect of silver nanoparticles prepared in glutathione mediated by green method, Chem. Cent. J. 8 (2014) 11, https://doi.org/10.1186/1752-153X-8-11.
[43] M.A. Awad, P. Virk, A.A. Hendi, K.M. Ortashi, N. AlMasoud, T.S. Alomar, Role of biosynthesized silver nanoparticles with trigonella foenum-graecum seeds in wastewater treatment, Processes 11 (2023) 2394, https://doi.org/10.3390/pr11082394.
[44] C.S. Wong, N.S. Bennett, D. Manessis, A. Danilewsky, P.J. McNally, Non-destructive laboratory-based X-ray diffraction mapping of warpage in Si die embedded in IC packages, Microelectron. Eng. 117 (2014) 48–56, https://doi.org/10.1016/j.mee.2013.12.020.
[45] A. Pandey, S. Dalal, S. Dutta, A. Dixit, Structural characterization of polycrystalline thin films by X-ray diffraction techniques, J. Mater. Sci. Mater. Electron. 32 (2021) 1341–1368, https://doi.org/10.1007/s10854-020-04998-w.

[46] M. Abo-Elmaaref, M. Marouf, W.S. Mohamed, W.A. Abdel Wahab, Antifungal and consolidation properties of linen textiles treated with silver nanoparticles loaded on hydroxypropyl cellulose polymer, Herit. Sci. 11 (2023) 120, https://doi.org/10.1186/s40494-023-00964-x.
[47] L. Sun, P.C. Lv, Y.C. Yin, H.N. Li, F. Wang, Green synthesis of silver nanoparticles using wolfberry fruits extract and their photocatalytic performance, IOP Conf. Ser. Mater. Sci. Eng. 292 (2018) 012017, https://doi.org/10.1088/1757-899X/292/1/012017.
[48] M. Fatemi, N. Mollania, M. Momeni-Moghaddam, F. Sadeghifar, Extracellular biosynthesis of magnetic iron oxide nanoparticles by Bacillus cereus strain HMH1: Characterization and in vitro cytotoxicity analysis on MCF-7 and 3T3 cell lines, J. Biotechnol. 270 (2018) 1–11, https://doi.org/10.1016/j.jbiotec.2018.01.021.
[49] A. Lateef, M.A. Akande, M.A. Azeez, S.A. Ojo, B.I. Folarin, E.B. Gueguim-Kana, L. S. Beukes, Phytosynthesis of silver nanoparticles (AgNPs) using miracle fruit plant (Synsepalum dulcificum) for antimicrobial, catalytic, anticoagulant, and thrombolytic applications, Nanotechnol. Rev. 5 (2016) 507–520, https://doi.org/10.1515/ntrev-2016-0039.
[50] V. Swetha, S. Lavanya, G. Sabeena, E. Pushpalaksmi, S.J. Jenson, G. Annadurai, Synthesis and characterization of silver nanoparticles from <I>Ashyranthus aspera< /I> extract for antimicrobial activity, Stud., J. Appl. Sci. Environ. Manag. 24 (2020) 1161–1167, https://doi.org/10.4314/jasem.v24i7.6.
[51] J.C. Ontong, S. Paosen, S. Shankar, S.P. Voravuthikunchai, Eco-friendly synthesis of silver nanoparticles using Senna alata bark extract and its antimicrobial mechanism through enhancement of bacterial membrane degradation, J. Microbiol. Methods 165 (2019) 105692, https://doi.org/10.1016/j.mimet.2019.105692.
[52] E. Avirdi, H.K. Paumo, B.P. Kamdem, M.B. Singh, K. Kumari, L. Katata-Seru, I. Bahadur, Imidazolium-based ionic liquid-assisted silver nanoparticles and their antibacterial activity: experimental and density functional theory studies, ACS Omega 8 (2023) 42976–42986, https://doi.org/10.1021/acsomega.3c06171.
[53] A. Toranzo, P.S. Bustos, M.G. Ortega, P.L. Páez, C. Lucero-Estrada, Biologically synthesized silver nanoparticles, mediated by *Bothriochloa laguroides*, inhibit biofilm formation and eradicate mature biofilm of *Yersinia enterocolitica* and *Staphylococcus aureus*, J. Appl. Microbiol. 132 (2022) 209–220, https://doi.org/10.1111/jam.15195.
[54] M. Jamal, W. Ahmad, S. Andleeb, F. Jalil, M. Imran, M.A. Nawaz, T. Hussain, M. Ali, M. Rafiq, M.A. Kamil, Bacterial biofilm and associated infections, J. Chin. Med. Assoc. 81 (2018) 7–11, https://doi.org/10.1016/j.jcma.2017.07.012.
[55] C.-H. Yang, P.-W. Su, S.-H. Moi, L.-Y. Chuang, Biofilm formation in acinetobacter baumannii: genotype-phenotype correlation, Molecules 24 (2019) 1849, https://doi.org/10.3390/molecules24101849.
[56] S.J. Kassinger, M.L. Van Hoek, Biofilm architecture: an emerging synthetic biology target, Synth. Syst. Biotechnol. 5 (2020) 1–10, https://doi.org/10.1016/j.synbio.2020.01.001.
[57] H. Barabadi, A. Mohammadzadeh, H. Vahidi, M. Rashedi, M. Saravanan, N. Talank, A. Alizadeh, Penicillium chrysogenum-derived silver nanoparticles: exploration of their antibacterial and biofilm inhibitory activity against the standard and pathogenic acinetobacter baumannii compared to tetracycline, J. Clust. Sci. 33 (2022) 1929–1942, https://doi.org/10.1007/s10876-021-02121-5.
[58] R. Singh, J. Vora, S.B. Nadhe, S.A. Wadhwani, U.U. Shedbalkar, B.A. Chopade, Antibacterial activities of bacteriagenic silver nanoparticles against nosocomial *Acinetobacter baumannii*, J. Nanosci. Nanotechnol. 18 (2018) 3806–3815, https://doi.org/10.1166/jnn.2018.15013.
[59] F. Xia, X. Tao, H. Wang, J. Shui, C. Min, Y. Xia, J. Li, M. Tang, Z. Liu, Y. Hu, H. Luo, M. Zou, Biosynthesis of silver nanoparticles using the biofilm supernatant of pseudomonas aeruginosa PA75 and evaluation of their antibacterial, antibiofilm, and antitumor activities, Int. J. Nanomed. 18 (2023) 2485–2502, https://doi.org/10.2147/IJN.S410314.
[60] C. De La Fuente-Núñez, V. Korolik, M. Bains, U. Nguyen, E.B.M. Breidenstein, S. Horsman, S. Lewenza, L. Burrows, R.E.W. Hancock, Inhibition of bacterial biofilm formation and swarming motility by a small synthetic cationic peptide, Antimicrob. Agents Chemother. 56 (2012) 2696–2704, https://doi.org/10.1128/AAC.00064-12.
[61] D. Roe, B. Karandikar, N. Bonn-Savage, B. Gibbins, J.-B. Roullet, Antimicrobial surface functionalization of plastic catheters by silver nanoparticles, J. Antimicrob. Chemother. 61 (2008) 869–876, https://doi.org/10.1093/jac/dkn034.
[62] S. Sharma, J. Mohler, S.D. Mahajan, S.A. Schwartz, L. Bruggemann, R. Aalinkeel, Microbial biofilm: a review on formation, infection, antibiotic resistance, control measures, and innovative treatment, Microorganisms 11 (2023) 1614, https://doi.org/10.3390/microorganisms11061614.
[63] R. Ma, X. Hu, X. Zhang, W. Wang, J. Sun, Z. Su, C. Zhu, Strategies to prevent, curb and eliminate biofilm formation based on the characteristics of various periods in one biofilm life cycle, Front. Cell. Infect. Microbiol. 12 (2022) 1003033, https://doi.org/10.3389/fcimb.2022.1003033.
[64] R Core Team. (2020). R: A language and environment for statistical computing. R Foundation for Statistical Computing, Vienna, Austria. URL: https://www.R-project.org/.